Indefinite dielectric response and all-angle negative refraction in a structure with deeply-subwavelength inclusions

Chandra S. R. Kaipa* and Alexander B. Yakovlev
Department of Electrical Engineering, The University of Mississippi, University, Mississippi 38677, USA

Stanislav I. Maslovski and Mário G. Silveirinha
Department of Electrical Engineering-Instituto de Telecomunicações, University de Coimbra - Pólo II, 3030-290 Coimbra, Portugal
(Received 4 August 2011; revised manuscript received 17 September 2011; published 28 October 2011)

The realization of mesoscopic media that mimic an ideal continuous indefinite material remains a challenging problem, particularly because current designs are plagued by spatial dispersion effects and are based on inclusions whose size may be a significant fraction of the wavelength. Here we show that a structure formed by an array of inductively loaded metallic rods terminated by metallic patches at both ends may enable to largely overcome these problems, and imitate more closely indefinite dielectric media with a local response. In particular, we report a strong all-angle negative refraction effect, even in scenarios where the characteristic size of the material is deeply subwavelength. The response of the proposed structure is characterized using a homogenization model developed for the uniaxial wire medium with impedance loadings.

DOI: 10.1103/PhysRevB.84.165135 PACS number(s): 78.66.Sq, 42.70.Qs, 78.20.Ci, 41.20.Jb

I. INTRODUCTION

Media exhibiting negative index or negative refraction effects[1] have been the subject of study in recent years due to their extraordinary and exotic properties - rooted in the complex interactions between their basic elements and radiation - which have stimulated the imagination of the scientific community. In particular, it was predicted that metamaterials may enable subwavelength imaging[2] and the realization of novel high-resolution lenses, and may also permit partial focusing with planar lenses. For the operation of such planar lenses, all-angle negative refraction and high transmission are often required. Although negative refraction is not observed in conventional dielectrics, the advent of metamaterials brought new opportunities to permit its occurrence, as reported in recent literature. For example, broadband negative refraction can be observed in a nonlocal material formed by crossed metallic wires,[3] and in photonic crystals with engineered dispersion.[4]

In Refs. 5–7, the negative refraction and partial focusing have been realized using indefinite materials with permittivity and permeability tensors having a different sign in the principal components. Besides their unusual refracting properties, materials with indefinite parameters have other interesting potentials stemming from their anomalously high density of electromagnetic states,[8,9] which can enable exciting effects such as broadband Purcell radiation. Hence, the realization and modeling of mesoscopic media with an indefinite dielectric response is a problem of increasing importance.

The obvious solution to realize a medium with indefinite properties with a local response is to consider an array of nanorods arranged in a crystal lattice. However, at microwaves and THz frequencies, the array of nanorods is typically characterized by strong spatial dispersion,[10] and it behaves very differently from a material with indefinite anisotropic permittivity. Despite these difficulties, it has been shown recently that by periodically attaching metallic patches to an array of metallic wires,[11,12] it is possible to dramatically reduce spatial dispersion (SD) effects[13–15] as originally suggested in Ref. 13. However, some residual spatial dispersion is still observed for wide incident angles, and in particular the designs considered in Refs. 11 and 12 do not exhibit all-angle negative refraction. It should be noted that the SD effects in the wire medium (WM) can also be reduced by coating the wires with a magnetic material or, equivalently, by increasing the inductance of the wires.[13]

In this work, we show that at microwaves and low THz frequencies the SD effects can be significantly reduced (even for wide incident angles) by loading the WM slab with impedance insertions (lumped inductive loads). Also, increasing the value of the inductive load reduces the plasma frequency and enables the design of an ultra thin structure with the electrical length of the unit cell being much smaller than that of the structure without the loads, at corresponding frequencies of operation. The proposed structure exhibits indefinite dielectric response, high transmission, and all-angle negative refraction below the plasma frequency, which is the main result of this paper. The analysis is carried out using different homogenization models[16,17] developed for the uniaxial WM loaded with conducting plates and (or) impedance insertions based on the quasistatic approach (which assume uniform and discrete loadings), and take into account the SD effects in the wires. The numerical results of the proposed configuration show a strong negative refraction with a near perfect transmission at microwaves.

The paper is organized as follows. In Sec. II, the formalism of the uniform-loading and discrete-loading homogenization models for the analysis of the loaded WM is presented. It is shown that there is a possibility to neglect the SD effects in the uniform-loading model which gives rise to a local model with Drude-type effective permittivity for the inductively loaded uniaxial WM. Section III focuses on the analysis of the proposed configuration with the plane-wave incidence and Gaussian beam excitation. In particular, the emergence of negative refraction in the ultra thin structure is numerically demonstrated. The conclusions are drawn in Sec. IV.

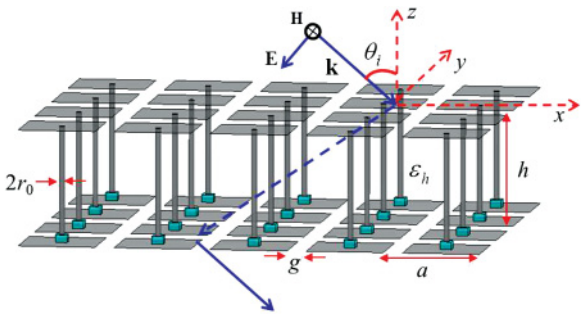

FIG. 1. (Color online) A 3D view of a two-sided mushroom structure with inductive loads at the wire-to-patch connections excited by an obliquely incident TM-polarized plane wave.

II. HOMOGENIZATION MODELS FOR LOADED WIRE MEDIUM

The configuration under study is shown in Fig. 1. The structure consists of an array of parallel conducting wires with radius r_0 directed along z in a host medium with relative permittivity ε_h. The patch arrays are at the planes $z = 0$ and $z = -h$, and the wires are connected to the metallic patches through lumped loads. The period of the square patches is a, and the gap is g. A time dependence of the form $e^{j\omega t}$ is assumed and suppressed.

In Sec. II A, we review the general expression for the spatially dispersive permittivity of a uniaxial continuously loaded wire medium. Based on this model, the interaction of electromagnetic waves with the structure of interest (Fig. 1) can be described using homogenization techniques with different levels of accuracy. One option is to consider that the effect of the lumped loads can be approximated by a distributed uniform loading. Within this framework, detailed in Sec. II B, the array of wires and lumped loads are regarded as a bulk material. Thus, the effective dielectric function includes the response of both the wires and lumped loads. In general the dielectric function of such a bulk medium depends on the wave vector, because of the effects of spatial dispersion. A simpler model can be obtained by discarding the dependence of the dielectric function on the wave vector. Such a local model is described in Sec. II C. Finally, a third option is to take into account the actual discreteness of lumped loads. Within this alternative and more accurate approach, the effect of the lumped load is not incorporated in the effective dielectric function of the material, but rather taken into account through suitable boundary conditions. This approach is discussed in Sec. II D.

A. Dielectric function for a continuously loaded wire medium

We model the wire medium using the quasistatic approach described in Ref. 16, which is formulated in terms of an effective capacitance and an effective inductance per unit length. The permittivity dyadic [Eq. (33), Ref. 16] of the uniaxial WM hosted in a medium with permittivity ε_h and uniformly loaded with metallic patches and (or) impedance insertions is expressed as follows:

$$\frac{\bar{\bar{\varepsilon}}}{\varepsilon_0} = \varepsilon_h \left[\varepsilon_t \bar{\bar{I}}_t + \left(1 - \frac{k_p^2}{k_h^2 - j\xi k_h - k_z^2/n^2} \right) \mathbf{z}_0 \mathbf{z}_0 \right], \quad (1)$$

where ε_t is the transverse permittivity[18] for the patch arrays separated by distance h, k_p is the plasma wave number of the WM defined in Ref. 16, $k_h = k_0\sqrt{\varepsilon_h}$ is the wave number in the host medium, $k_0 = \omega/c$ is the free space wave number, k_z is the wave vector component along $\mathbf{z}_0$, and $\bar{\bar{I}}_t$ is the unit dyadic in the plane orthogonal to $\mathbf{z}_0$.

In Eq. (1), $n^2 = LC/(\varepsilon_h \varepsilon_0 \mu_0)$ is the square of the slow-wave factor, which determines the degree of nonlocality of the material's response. The larger is n, the less important are the effects of spatial dispersion. The value of n is minimal when the wires are unloaded and stand in vacuum, and in that case $n = 1$. In practice, the value of n can be tuned by loading the wires with suitable loads. In the above expression for the slow-wave factor, L is the effective inductance per unit length of a wire in the WM as defined in Ref. 19, $C = C_{\text{wire}} + C_{\text{patch}}/h$ is the effective capacitance per unit length of a wire in the WM loaded with metallic patches as defined in Ref. 16, $\xi = (Z_w/L)\sqrt{\varepsilon_h \varepsilon_0 \mu_0}$, and Z_w is the self-impedance per unit length of a wire, which may include the effect of lumped elements. When the losses in the metal are negligible (as assumed in this work) and the effect of the lumped loads is incorporated in the dielectric function, we have $Z_w = Z_{\text{Load}}/h$, where Z_{Load} accounts for the type of the lumped load (inductive/capacitive). The explicit formulas for the notations in Eq. (1) and for those discussed above are given in Appendix A.

The quasistatic model of Ref. 16 does not take into account the granularity of the structure along z, i.e., the loading is assumed to be effectively continuous along the wires. In Ref. 17, this model has been improved to account for discontinuities in the distributions of wire current and charge at the points of lumped insertions. In what follows, we describe the homogenization models resulting from the studies of Refs. 16 and 17, and in Sec. III apply them to the analysis of transmission properties in the indefinite dielectric media.

B. Uniform loading within period

Ignoring loading by the patches ($\varepsilon_t = 1$ and $C = C_{\text{wire}}$) and assuming that each period of the uniaxial WM is loaded with lumped inductance L_1 (with an impedance $Z_{\text{Load}} = j\omega L_1$), we may include the load impedance into the self-impedance of the wire, obtaining, when the loss in wires is neglected, $Z_w = Z_{\text{Load}}/h$. Then, the relative permittivity along $\mathbf{z}_0$ in Eq. (1), after substituting all the intermediate quantities and doing a simplification, can be expressed as

$$\frac{\varepsilon_{zz}}{\varepsilon_0} = \varepsilon_h \left(1 - \frac{\tilde{k}_p^2}{k_h^2 - k_z^2/\tilde{n}^2} \right). \quad (2)$$

Here, $\tilde{k}_p = k_p/\sqrt{1 + L_1/(hL)}$ is the effective plasma wave number and $\tilde{n} = n\sqrt{1 + L_1/(hL)}$ is an effective slow-wave factor. Alternatively, the same result can also be obtained if the loading inductance is included directly into the wire inductance per unit length: $\tilde{L} = L + L_1/h$, so that $\tilde{n}^2 = \tilde{L}C_{\text{wire}}/(\varepsilon_h \varepsilon_0 \mu_0)$ and $\tilde{k}_p = \sqrt{\mu_0/(a^2\tilde{L})}$. It can be inferred from Eq. (2) that with an increase in the value of the lumped inductance we have a decrease in the plasma frequency and a dramatic reduction in the spatial dispersion effects. It should be noted that this simple approach treats the inductive insertions as uniform loadings over the period, therefore the discontinuity in the

charge distribution close to the point where an inductor is inserted is neglected. However, even such a simplified model may give physical insight on the effects of spatial dispersion in the loaded WM.

In accordance with Ref. 17, the discontinuities in the wire current distribution $I(z)$ at the points where the wires meet the patches are taken into account in this model by the following additional boundary condition (ABC):

$$\left[\frac{dI(z)}{dz} \pm \frac{C_{\text{wire}}}{C_{\text{patch}}} I(z)\right]_{z=0,-h} = 0, \tag{3}$$

with the plus sign used at $z = 0$, and the minus sign at $z = -h$. When $a \approx h$ and $g \ll a$, $C_{\text{patch}} \gg hC_{\text{wire}}$ and this ABC reduces to the one used in Ref. 14. In addition to this, to account for the discontinuity in the tangential magnetic field at the two sides of the patch arrays, these arrays are modeled with the sheet admittance[20]

$$Y_g = j(\varepsilon_h + 1)\frac{k_0 a}{\pi \eta_0} \log\left[\csc\left(\frac{\pi g}{2a}\right)\right]. \tag{4}$$

C. Local model

When $\tilde{n} \gg 1$ the spatial dispersion in the loaded WM is negligible, and the material can be described with a Drude-type local uniaxial permittivity. In this model, the relative permittivity along $\mathbf{z}_0$ for the WM slab loaded with lumped inductances is obtained from Eq. (2) by neglecting the wave-vector dependence of the permittivity, resulting in:

$$\frac{\varepsilon_{zz}^{\text{loc}}}{\varepsilon_0} = \varepsilon_h\left(1 - \frac{\tilde{k}_p^2}{k_h^2}\right), \tag{5}$$

with all the notations as defined in Sec. II A. This model treats the WM slab with inductive loadings as a local Epsilon Negative (ENG) continuous material, and takes into account only the frequency dispersion. Since the local model does not take into consideration the SD effects in the WM, it does not account for the discontinuities in the wire current distribution $[I(z)]$, and, therefore, does not require the use of ABC at the wire-to-patch connections.

Following Ref. 12, the transmission and reflection properties for the structure shown in Fig. 1 can be obtained in a similar way by matching the tangential electric and magnetic fields with the sheet impedance boundary conditions at the air-patch interfaces [with the admittance of the patch arrays given by Eq. (4)]. It should be noted that the local model predicts accurately the response of the structure when the SD effects in the inductively loaded WM are significantly reduced (we show in Sec. III that this is the case in the considered structured WM).

D. Discrete loading within period

The model from Sec. II B can be further improved by taking into account the precise position of the inductive load, so that this loading is not considered uniform over the period anymore. Using the results of Ref. 17 [or alternatively Eq. (1) with $n = 1$ and $\xi = 0$], the WM slab as a uniaxial medium (for long wavelengths) is characterized by relative effective permittivity

$$\frac{\bar{\bar{\varepsilon}}}{\varepsilon_0} = \varepsilon_h\left[\bar{\bar{I}}_t + \left(1 - \frac{k_p^2}{k_h^2 - k_z^2}\right)\mathbf{z}_0\mathbf{z}_0\right]. \tag{6}$$

As in Sec. II B, the WM slab is loaded with the metallic patch arrays at the planes $z = 0$ and $z = -h$ characterized by the sheet admittance given by Eq. (4). The impedance insertions (lumped inductive loads) are placed at the wire-to-patch connection at the plane $z = -h$ (see Fig. 1).

This model takes into account the spatial dispersion effects in the WM by considering that the field in the WM region is a superposition of the three fundamental plane wave modes of the bulk WM. Moreover, the nonlocal response of WM is taken into account by matching the fields at the patch interfaces through the known boundary conditions at an impedance sheet and applying the generalized additional boundary condition (GABC) for the wire current $I(z)$ at the connection of the lumped loads to the metallic elements (patches):[17]

$$\left[\frac{dI(z)}{dz} - \left(j\omega C_{\text{wire}} Z_{\text{Load}} + \frac{C_{\text{wire}}}{C_{\text{patch}}}\right) I(z)\right]_{z=-h} = 0. \tag{7}$$

The ABC at $z = 0$ is given by Eq. (3). The microscopic current $I(z)$ along the metallic wires can be written in terms of the bulk electromagnetic fields using the results of Ref. 17. The explicit expressions for the GABC and ABC in terms of the macroscopic electromagnetic fields are given in Appendix B. In the next section, the predictions of the developed analytical models are presented along with the numerical full-wave results.

III. RESULTS AND DISCUSSION

As a first step, in order to validate the homogenization models (uniform-loading and discrete-loading), we consider a scattering problem where an obliquely incident transverse magnetic (TM) plane wave illuminates a structured material slab with the following dimensions: $a = 2$ mm, $g = 0.2$ mm, $h = 2$ mm, $r_0 = 0.05$ mm, $\varepsilon_h = 10.2$, $\theta_i = 60^\circ$, and $L_1 = 0.2$ nH. The transmission and reflection properties for the structure shown in Fig. 1 can be obtained by writing the fields in the WM region as a superposition of the plane-wave modes determined by the permittivity functions for the uniform-loading model [Eq. (2)] and the discrete-loading model [Eq. (6)], and by matching the tangential electric and magnetic fields at the air-patch interfaces using the two-sided impedance boundary conditions. Also, both the models require the use of ABC [Eq. (3)] at the connection of the metallic wires to the patches. Additionally, discrete-loading model requires a GABC [Eq. (7)] at the connection of lumped loads to metallic patches. It should be noted that the uniform-loading and discrete-loading models presented here can in general be applied to any type of load (deeply-subwavelength inclusions). However, in the present work, we focus our attention only on the inductive loads.

The transmission properties (magnitude and phase) of the structure obtained from the uniform-loading model, discrete-loading model, and the local model are shown in Fig. 2. It is seen that the results of the three models are in a reasonable

agreement with the full-wave results obtained with HFSS,[21] except for a small shift in the frequency corresponding to the plasma resonance. However, the results of the local model show spurious resonances in a very narrow frequency band in the vicinity of the plasma frequency where $\varepsilon_{zz}^{\mathrm{loc}} = 0$. In the full-wave simulations, it is assumed that the load is connected to the patch through a gap of 0.1 mm. In practice, the insertion of a load introduces nonuniformities in the current and the charge distributions, therefore, the correction terms describing the parasitic inductance L_{par} and parasitic capacitance C_{par} should be taken into account in the expression for the load impedance.[17] However, for simplicity in the present work we ignore the effect of the parasitic elements because it is rather small. From Fig. 2, the plasma frequency is 10.6 GHz, which is reduced when compared to the case of no impedance insertions (short circuit) with the plasma frequency of 12.14 GHz. This confirms that by using the lumped inductances, we have a decrease in the plasma frequency. Moreover, the fact that the response of the local model is close to that of the full-wave simulations confirms that the effects of spatial dispersion are negligible. In the rest of the paper, we employ the discrete-loading model to study the transmission properties and to characterize the negative refraction.

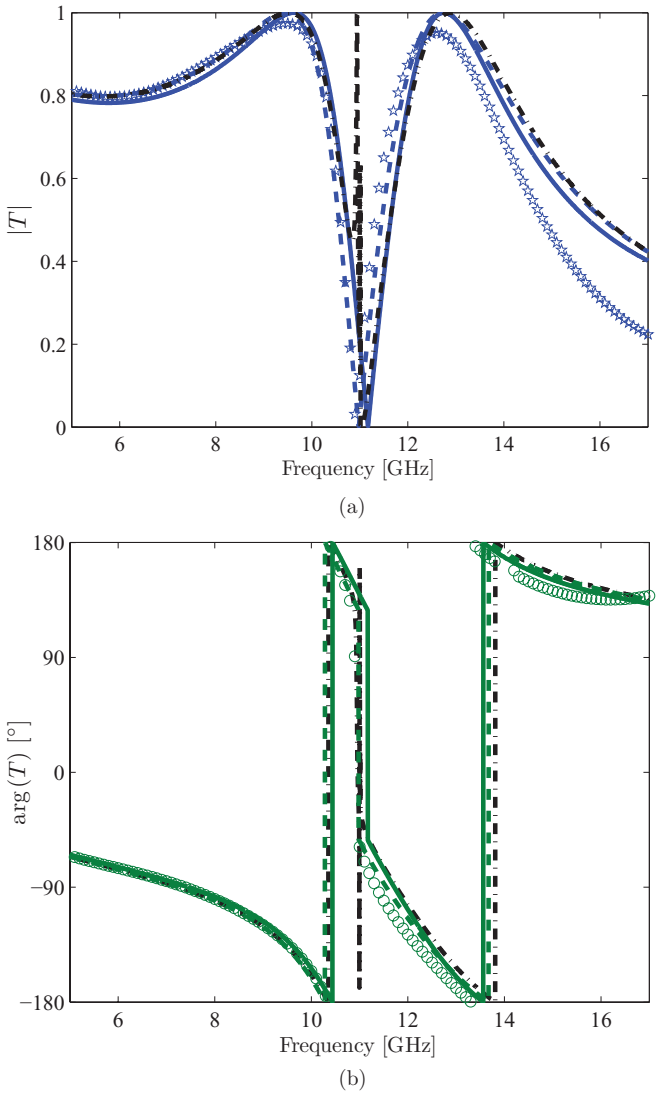

FIG. 2. (Color online) Transmission characteristics for the two-sided mushroom structure excited by a TM-polarized plane wave incident at 60° as a function of frequency. (a) Magnitude of the transmission coefficient. (b) Phase of the transmission coefficient. The solid lines represent the results of the uniform-loading model, the dashed lines are the discrete-loading model results, the dot-dashed lines are the local model results, and the symbols correspond to the full-wave HFSS results.

Now, we fix the plasma frequency (12.1 GHz) and increase the inductive load L_1 and decrease the permittivity ε_h of the structure simultaneously, with a motive to have a smaller unit cell at the frequency of operation and better transmission characteristics. Thus, the formed structure is of the following dimensions: $a = 2$ mm, $g = 0.2$ mm, $h = 2$ mm, $r_0 = 0.05$ mm, $\varepsilon_h = 1$, and $L_1 = 5$ nH. The transmission characteristics (magnitude and phase) of the structure obtained from the discrete-loading model for a TM-polarized plane wave incident at 60 degrees are depicted in Fig. 3(a). It can be seen that the homogenization results are in a good agreement with the full-wave HFSS results. It is assumed that the load is connected to the patch through a gap of 0.1 mm. The good agreement between simulations and theory reveals that the effects of the parasitic inductance and capacitance are negligible in the considered configuration, and justifies why these were not taken into account in our model. It can be observed from Fig. 3(a) that we have a better transmission magnitude (due to improved matching) when compared to the results in Fig. 2. The percentage decrease in the plasma frequency of the proposed configuration when compared to the structure without the inductive loads is nearly 66%.

Next, we characterize the negative refraction based on the analysis of variation in the phase of $T(\omega,k_x)$ (transmission coefficient for a plane wave with the transverse wave number k_x) of the material slab with the incident angle θ_i. Specifically, it was shown in Ref. 3 that for an arbitrary material slab excited by a quasiplane wave, apart from the transmission magnitude, the field profile at the output plane differs from the same at the input plane by a spatial shift Δ [see inset in Fig. 3(b)], given by $\Delta = d\phi/dk_x$, where $\phi = \arg(T)$. The transmission angle can be obtained as $\theta_t = \tan^{-1}(\Delta/h)$ (h is the thickness of the planar material slab). Thus, negative refraction occurs when $\Delta < 0$, i.e., when ϕ decreases with the angle of incidence θ_i.

The homogenization model results of the transmission magnitude and phase as a function of the incidence angle θ_i calculated at a frequency of 11 GHz are depicted in Fig. 3(b), showing a very good agreement with the full-wave CST Microwave Studio[22] results. It can be observed that the phase of the transmission coefficient [$\phi = \arg(T)$] decreases with an increase in the incidence angle, except at large incidence angles where we have a rapid variation in the magnitude of $T(\omega,k_x)$. This clearly shows that the structure enables negative refraction. The spatial shift calculated at an incident angle of 33.3° corresponding to the maximum transmission is $\Delta = -0.16\lambda_0$ (λ_0 is the free space wavelength calculated at 11 GHz). The electrical thickness of the structure is $h = 0.073\lambda_0$, and the calculated transmission angle is $\theta_t = -65.42°$. It is interesting that in spite of the structure being electrically very thin, it exhibits strong negative refraction at an interface with air. In order to further characterize the negative

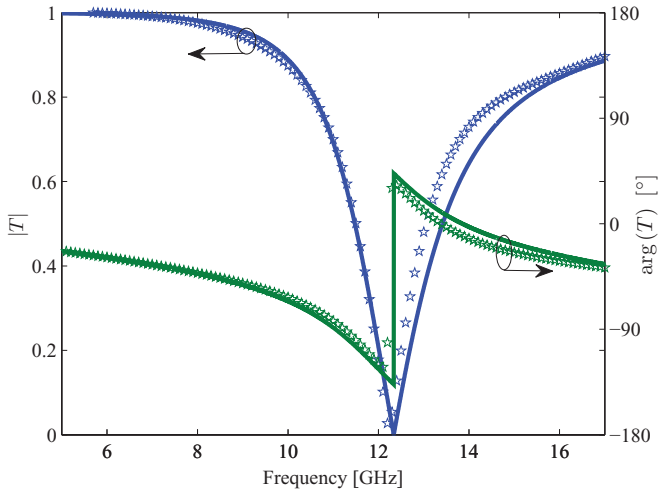

(a)

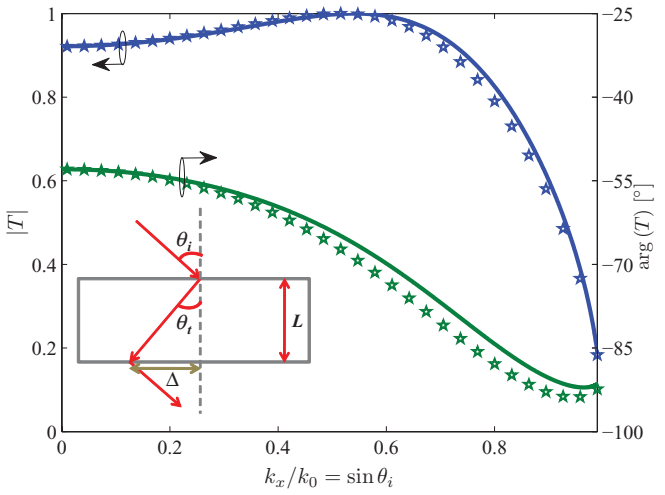

(b)

FIG. 3. (Color online) (a) The magnitude and phase of the transmission coefficient for the two-sided mushroom structure excited by a TM-polarized plane wave incident at 60° as a function of frequency. The solid lines represent the homogenization results, and the symbols correspond to the full-wave HFSS results. (b) Transmission magnitude and phase as a function of the incidence angle θ_i calculated at 11 GHz. The solid lines represent the homogenization results, and the symbols correspond to the full-wave CST Microwave Studio results.

refraction effect, we have calculated the transmission angle θ_t as a function of incidence angle θ_i at different frequencies. The calculations are based on the discrete-loading model and are depicted along with the transmission magnitude $|T|$ in Fig. 4. The results of the homogenization model predict an all-angle negative refraction with a maximum transmission, which is observed in the frequency band from 8.7 GHz to 10.8 GHz. The proposed structure is electrically very thin ($< \lambda_0/15$) in this frequency range.

To further confirm these findings based on the discrete-loading model, we have simulated the response of the proposed configuration excited by a cylindrical Gaussian beam using CST Microwave Studio. The Gaussian beam has magnetic field polarized along the y direction and $\theta_i = 33.3°$. The array

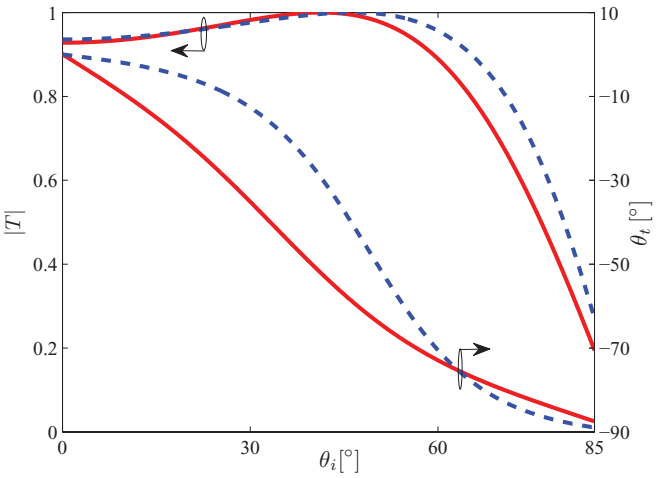

FIG. 4. (Color online) Discrete-loading model results of the transmission magnitude $|T|$ and the transmission angle θ_t as a function of the incidence angle θ_i calculated at different frequencies. The red solid lines and blue dashed lines correspond to the results calculated at 10 GHz and 9 GHz, respectively.

of loaded wires with patches has the same unit cell as that used in the calculations in Fig. 3(a). Both the Gaussian beam and the array are invariant to translations along y, and the width of the array along the x direction is $90a$. A snapshot in time of the

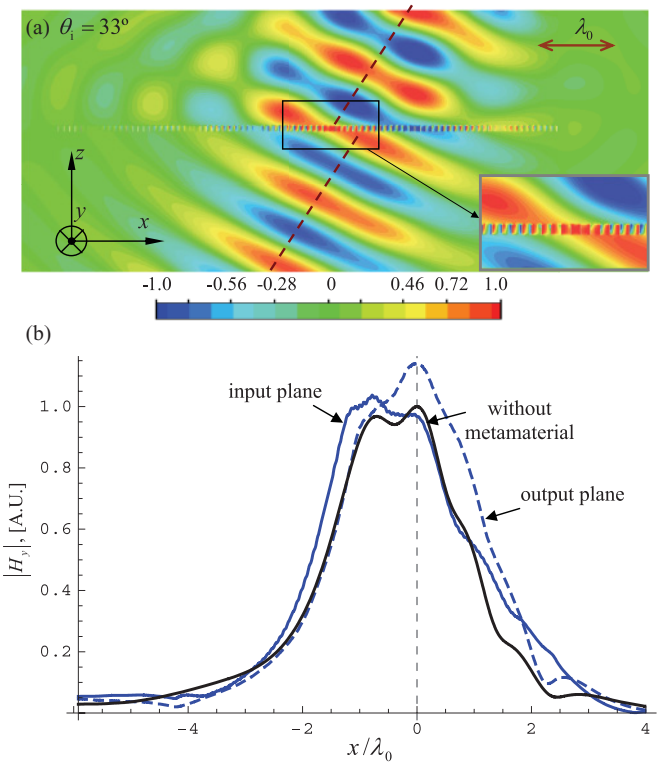

FIG. 5. (Color online) (a) Snapshot in time of the magnetic field H_y when the array of loaded wires is illuminated by a Gaussian beam with $\theta_i = 33°$. The inset shows a zoom of the central region of the structure. (b) Amplitude of the magnetic field in arbitrary units (a.u.) calculated at (i) Solid blue curve: input plane, (ii) dashed blue curve: output plane, and (iii) black curve: similar to (i) but for propagation in free space.

magnetic field at $t = 0$ is shown in Fig. 5(a) for $f = 11$ GHz, and the negative spatial shift of the incoming beam as it travels through the deeply-subwavelength array of loaded wires with patches is quite evident. In Fig. 5(b), we show the beam profile at a distance $0.5a$ above the input interface (blue solid curve) and at a distance $0.5a$ below the output interface (blue dashed curve). As a reference, we have also plotted the beam profile when the array is removed, and the Gaussian beam travels in free space (black curve, calculated at the same plane as the solid blue curve). Based on these profiles, it is possible to obtain the spatial shift by calculating the position of the center of mass of each curve (with weight $|H_y|^2$), and then the angle of transmission to the array of wires: $\theta_t \approx -75.5^\circ$.

IV. CONCLUSION

We have shown that by loading the WM slab with inductive loads, it is possible to decrease the plasma frequency of the uniaxial WM and reduce the spatial dispersion effects. By using the proposed concept of lumped loads, we have demonstrated that it is feasible to design an ultra-thin structure which exhibits all-angle negative refraction with a high transmission, the response of which can be accurately predicted by the developed homogenization model. The proposed structure can be used for focusing of waves and in the design of planar lenses because of its two very important properties: all-angle negative refraction and high transmission.

APPENDIX A

Here, we give the explicit formulas for the notations used in Eq. (1), and also for those described in Sec. II A, as defined in Ref. 16,

$$\begin{aligned} \varepsilon_t &= 1 + (2(a-g)/\pi h)\log[\csc(\pi g/2a)], \\ k_p &= \sqrt{(2\pi/a^2)/\log[a^2/(4r_0(a-r_0))]}, \\ L &= (\mu_0/2\pi)\log[a^2/(4r_0(a-r_0))], \\ C_{\text{wire}} &= 2\pi\varepsilon_h\varepsilon_0/\log[a^2/(4r_0(a-r_0))], \\ C_{\text{patch}} &= \pi\varepsilon_0(\varepsilon_h+1)(a-g)/\log[\sec(\pi g/2a)]. \end{aligned} \tag{A1}$$

APPENDIX B

For the discrete-loading model defined in Sec. II D, assuming that a TM-polarized plane wave propagating in the x–z plane is incident at an angle θ_i on the configuration shown in Fig. 1, the electric and magnetic fields in the air region above the structure ($z > 0$) can be expressed as

$$\begin{aligned} H_y &= e^{\gamma_0 z} - Re^{-\gamma_0 z}, \\ E_x &= \frac{-\gamma_0}{j\omega\varepsilon_0}[e^{\gamma_0 z} + Re^{-\gamma_0 z}], \end{aligned} \tag{B1}$$

where R is the reflection coefficient, $\gamma_0 = \sqrt{k_x^2 - k_0^2}$, and $k_x = k_0 \sin\theta_i$ is the x component of the wave vector $\mathbf{k}$. The fields in the WM region ($-h < z < 0$) can be expressed in terms of the TM and transverse electromagnetic (TEM) plane-wave modes of bulk wire media determined by the permittivity function [Eq. (6)]:

$$\begin{aligned} H_y = {} & A_{\text{TM}}^{+}e^{\gamma_{\text{TM}}(z+h)} + A_{\text{TM}}^{-}e^{-\gamma_{\text{TM}}(z+h)} \\ & + B_{\text{TEM}}^{+}e^{\gamma_{\text{TEM}}(z+h)} + B_{\text{TEM}}^{-}e^{-\gamma_{\text{TEM}}(z+h)}, \\ E_x = {} & \frac{j}{\omega\varepsilon_0\varepsilon_h}[\gamma_{\text{TM}}(A_{\text{TM}}^{+}e^{\gamma_{\text{TM}}(z+h)} - A_{\text{TM}}^{-}e^{-\gamma_{\text{TM}}(z+h)}) \\ & + \gamma_{\text{TEM}}(B_{\text{TEM}}^{+}e^{\gamma_{\text{TEM}}(z+h)} - B_{\text{TEM}}^{-}e^{-\gamma_{\text{TEM}}(z+h)})], \\ E_z = {} & -\frac{k_x\eta_0}{k_0\varepsilon_{zz}^{\text{TM}}}(A_{\text{TM}}^{+}e^{\gamma_{\text{TM}}(z+h)} + A_{\text{TM}}^{-}e^{-\gamma_{\text{TM}}(z+h)}), \end{aligned} \tag{B2}$$

where $\gamma_{\text{TM}} = \sqrt{k_x^2 + k_p^2 - k_0^2\varepsilon_h}$, $\gamma_{\text{TEM}} = jk_0\sqrt{\varepsilon_h}$, and $\varepsilon_{zz}^{\text{TM}} = \varepsilon_h k_x^2/(k_p^2 + k_x^2)$ is the relative permittivity along the wires for TM polarization. $A_{\text{TM}}^{\pm}$ and $B_{\text{TEM}}^{\pm}$ are the unknown amplitudes associated with the TM and TEM fields in the WM slab, respectively. The tangential electromagnetic fields in the air region below the structure ($z < -h$) are written as

$$H_y = Te^{\gamma_0(z+h)}, \quad E_x = \frac{-\gamma_0}{j\omega\varepsilon_0}Te^{\gamma_0(z+h)}, \tag{B3}$$

where T is the transmission coefficient. Now, the ABC [Eq. (3) at $z = 0$] and GABC [Eq. (7) at $z = -h$] can be written in terms of the field quantities, by expressing the microscopic current $I(z)$ along the wires in terms of the macroscopic electromagnetic fields using the results of Ref. 17:

$$\left[\left(k_0\varepsilon_h\frac{dE_z}{dz} + k_x\eta_0\frac{dH_y}{dz}\right) + \frac{C_{\text{wire}}}{C_{\text{patch}}}(k_0\varepsilon_h E_z + k_x\eta_0 H_y)\right]_{z=0} = 0, \tag{B4}$$

$$\left[\left(k_0\varepsilon_h\frac{dE_z}{dz} + k_x\eta_0\frac{dH_y}{dz}\right) - \left(j\omega C_{\text{wire}}Z_{\text{Load}} + \frac{C_{\text{wire}}}{C_{\text{patch}}}\right) \times (k_0\varepsilon_h E_z + k_x\eta_0 H_y)\right]_{z=-h} = 0. \tag{B5}$$

*ckaipa@olemiss.edu

[1] V. G. Veselago, Sov. Phys. USP. **10**, 509 (1968).
[2] J. B. Pendry, Phys. Rev. Lett. **85**, 03966 (2000).
[3] M. G. Silveirinha, Phys. Rev. B **79**, 153109 (2009).
[4] E. Cubukcu, K. Aydin, E. Ozbay, S. Foteinopoulou, and C. M. Soukoulis, Nature (London) **423**, 604 (2003).
[5] D. R. Smith and D. Schurig, Phys. Rev. Lett. **90**, 077405 (2003).
[6] D. R. Smith, D. Schurig, J. J. Mock, P. Kolinko, P. Rye, and Appl. Phys. Lett. **84**, 2244 (2004).
[7] Q. Cheng, R. Liu, J. J. Mock, T. J. Cui, and D. R. Smith, Phys. Rev. B **78**, 121102 (2008).

[8]Z. Jacob, I. Smolyaninov, and E. Narimanov, e-print arXiv:0910.3981v2.
[9]Z. Jacob, J.-Y. Kim, G. Naik, A. Boltasseva, E. Narimanov, and V. Shalaev, Appl. Phys. B **100**, 215 (2010).
[10]P. A. Belov, R. Marques, S. I. Maslovski, I. S. Nefedov, M. Silveirinha, C. R. Simovski, and S. A. Tretyakov, Phys. Rev. B **67**, 113103 (2003).
[11]M. G. Silveirinha and A. B. Yakovlev, Phys. Rev. B **81**, 233105 (2010).
[12]C. S. R. Kaipa, A. B. Yakovlev, and M. G. Silveirinha, J. Appl. Phys. **109**, 044901 (2011).
[13]A. Demetriadou and J. B. Pendry, J. Phys. Condens. Matter **20**, 295222 (2008).
[14]O. Luukkonen, M. G. Silveirinha, A. B. Yakovlev, C. R. Simovski, I. S. Nefedov, and S. A. Tretyakov, IEEE Trans. Microwave Theory Tech. **57**, 2692 (2009).
[15]A. B. Yakovlev, M. G. Silveirinha, O. Luukkonen, C. R. Simovski, I. S. Nefedov, and S. A. Tretyakov, IEEE Trans. Microwave Theory Tech. **57**, 2700 (2009).
[16]S. I. Maslovski and M. G. Silveirinha, Phys. Rev. B **80**, 245101 (2009).
[17]S. I. Maslovski, T. A. Morgado, M. G. Silveirinha, C. S. R. Kaipa, and A. B. Yakovlev, New J. Phys. **12**, 113047 (2010).
[18]S. A. Tretyakov, *Analytical Modelling in Applied Electromagnetics* (Artech House, Norwood, MA, 2003).
[19]S. I. Maslovski, S. A. Tretyakov, and P. A. Belov, Microw. Opt. Techn. Lett. **35**, 47 (2002).
[20]O. Luukkonen, C. R. Simovski, G. Granet, G. Goussetis, D. Lioubtchenko, A. V. Raisanen, and S. A. Tretyakov, IEEE Trans. Antennas Propagat. **56**, 1624 (2008).
[21]HFSS: High Frequency Structure Simulator based on Finite Element Method, Ansoft Corporation [http://www.ansoft.com].
[22]CST Microwave Studio 2011, CST GmbH [http://www.cst.com].